

Supporting Information

Modulating the Residual Ammonium in MnO₂ for High-Rate Aqueous Zinc-ion Battery

Yancheng Fu,^a Caoer Jia,^a Zihan Chen,^a Xiaosheng Zhang,^a Shuaijie Liang,^a Zhen Zhai,^a Jinzhou Chen,^a Xuying Liu,^a Linlin Zhang^{*a,b}

Y. Fu, C. Jia, Z. Chen, X. Zhang, S. Liang, Prof. J. Chen, Prof. X. Liu, Ass. Prof. L. Zhang
The Key Laboratory of Material Processing and Mold of Ministry of Education, Henan Key Laboratory of Advanced Nylon Materials and Application, School of Materials Science and Engineering, Zhengzhou University, Zhengzhou 450001, P. R. China

Ass. Prof. L. Zhang

The Key Laboratory of Advanced Energy Materials Chemistry (Ministry of Education), College of Chemistry, Nankai University, Tianjin 300071, P. R. China

E-mail: zhangll@zzu.edu.cn

1. Supporting figures and table

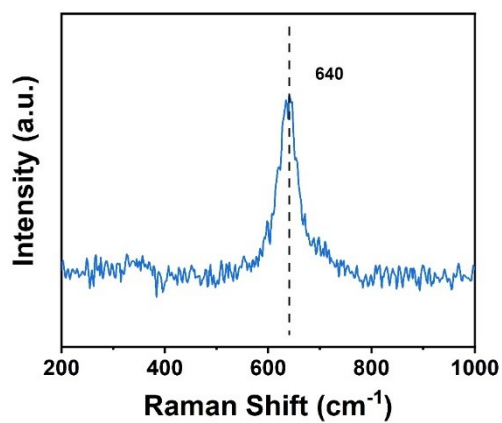


Fig. S1. Raman shift spectrum of NMO.

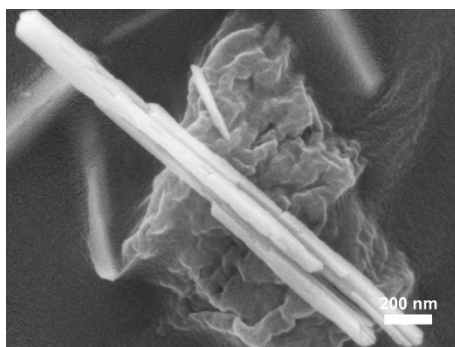


Fig. S2. The corresponding SEM image of NMO.

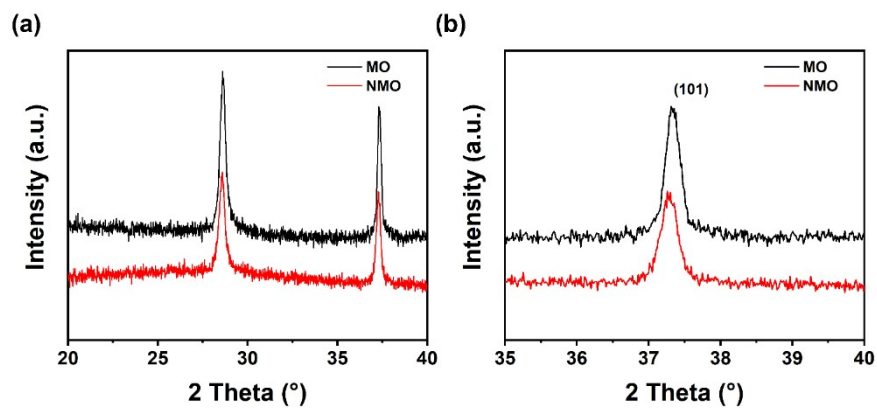


Fig. S3. XRD patterns of NMO and MO materials.

With the residual NH_4^+ in MnO_2 , the interlayer distance of MnO_2 increases from 0.31 nm to 0.32 nm in the plane (110) and from 0.24 nm to 0.25 nm in the plane (101), as illustrated in Fig. S3, demonstrating that the NH_4^+ extending the interlayer distance.

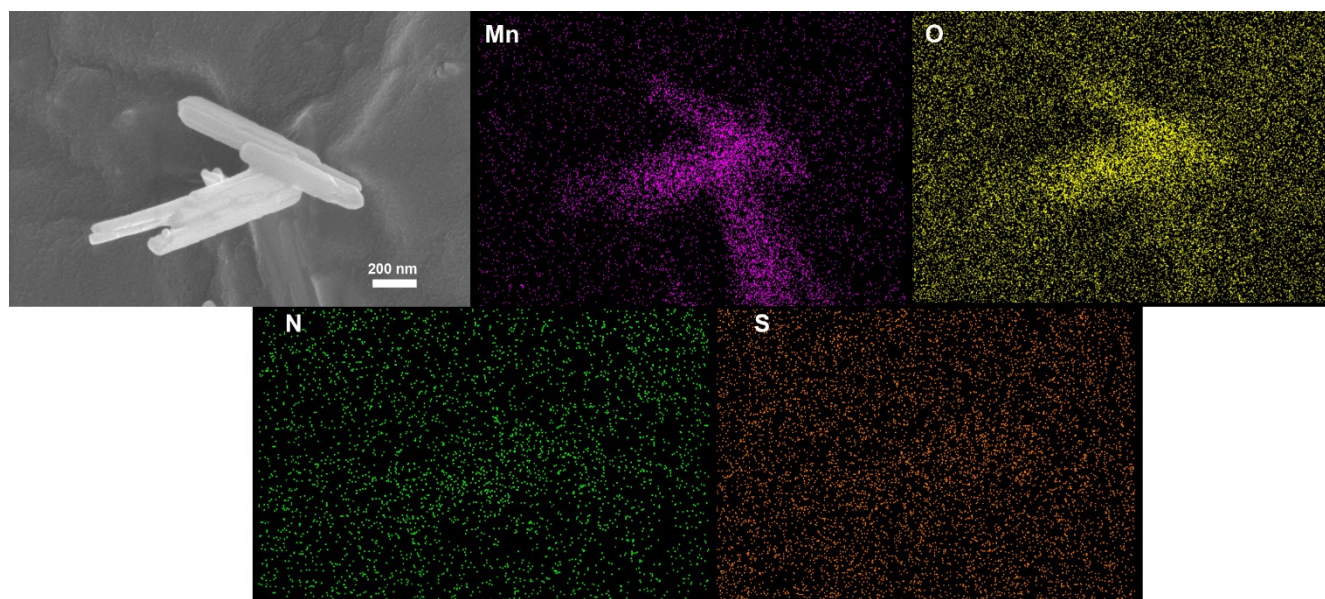


Fig. S4. SEM image of MO and its element mappings of Mn, O, N and S elements.

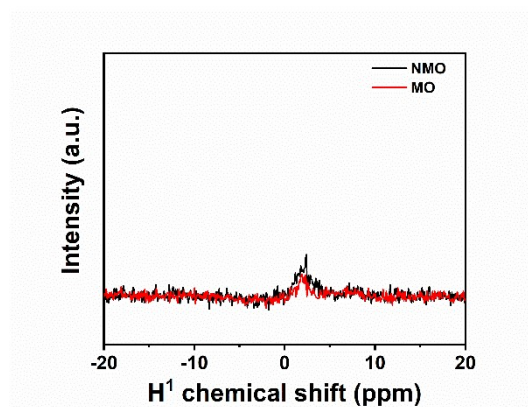


Fig. S5. Solid state ^1H NMR of NMO (black line) and MO (red line).

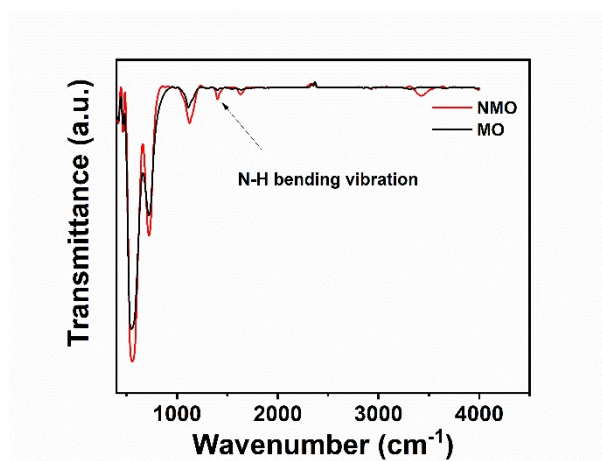


Fig. S6. FT-IR spectra of NMO (black line) and MO (red line) powder.

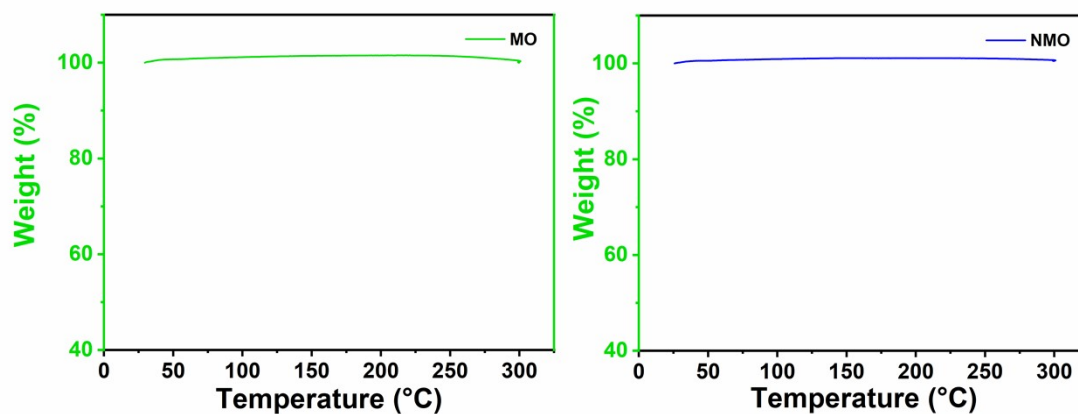


Fig. S7. TGA curves of MO and NMO.

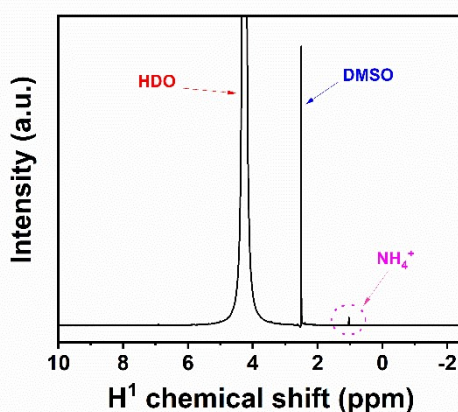


Fig. S8. ¹H NMR of the supernatant electrolyte (after soaking NMO for 24 h).

According to the experimental section, the residual NH₄⁺ could be washed by a large amount of deionized water to obtain pure MnO₂ without NH₄⁺. Herein, we firstly put the fabricated NMO powder into deionized water after soaking for 24 h. Then, the supernatant was characterized by the ¹H NMR. As displayed in Fig. S8, there are three obvious characteristic peaks, including two peaks with high intensity and one weak peak. The two peaks with high intensity are ascribed to HDO and DMSO, respectively. And the weak peak is H derived from the NH₄⁺, which represents the NH₄⁺ in MnO₂ dissolved in deionized water after soaking for 24 h. It directly confirms the existence of NH₄⁺ in MnO₂.

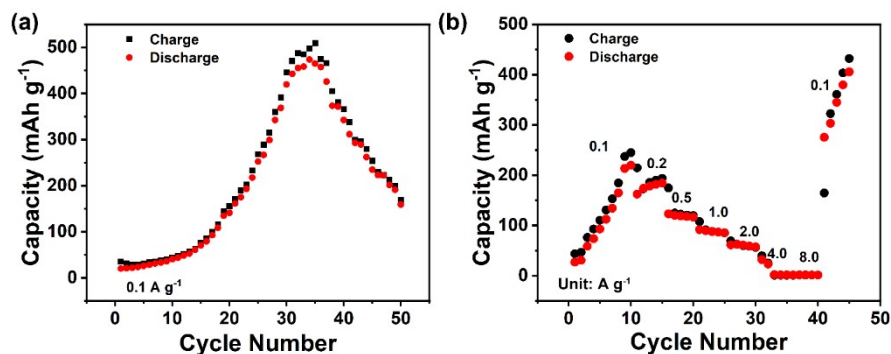


Fig. S9. The electrochemical performance of the battery assembled without NMO electrode.

The battery delivers a capacity of 509.6 mAh g^{-1} at 35th cycle, as shown in Fig. S9. The higher capacity comes from the electro-oxidation of Mn^{2+} in aqueous mixed electrolyte (1 M ZnSO_4 and 0.1 M MnSO_4). Therefore, the highest capacity in Figure 2e reaches $\sim 800 \text{ mAh g}^{-1}$ could be attributed to the electro-oxidation of Mn^{2+} in aqueous electrolyte. In addition, the rate performance of the battery could also confirm the electro-oxidation of Mn^{2+} in charge/discharge process. Moreover, with the increasing current densities, the contribution of Mn^{2+} in capacity decreases and could also recover when the current density returns to 0.1 A g^{-1} , which also confirm the cycle stability of electrolyte in electrochemical process.

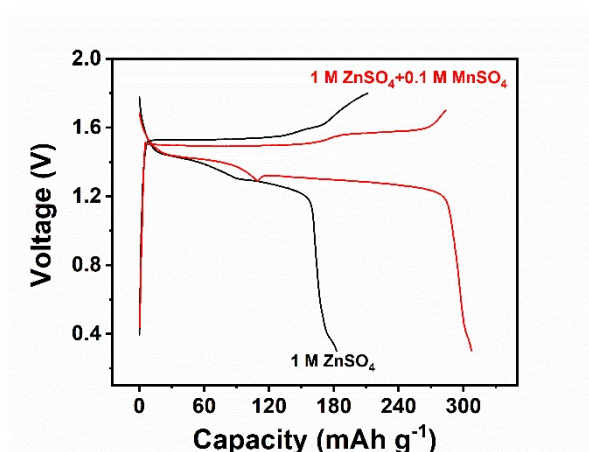


Fig. S10. Comparison of NMO's performance in different electrolyte at current density of 0.1 A g^{-1} .

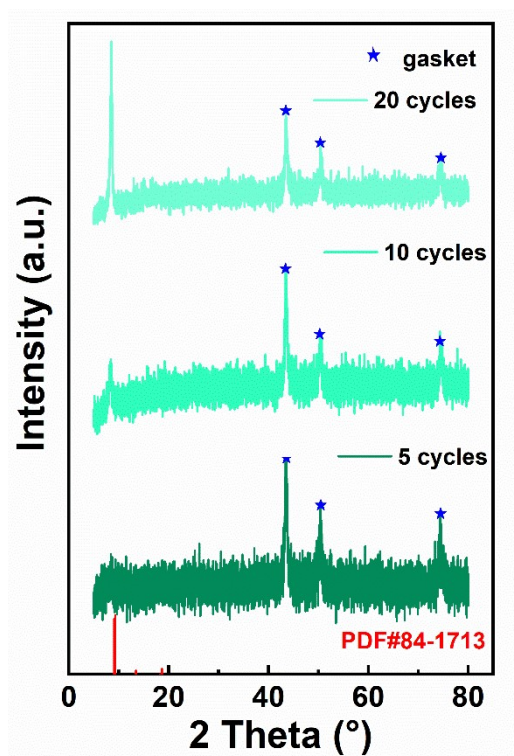


Fig. S11. The XRD patterns of gasket at cathode position at 5th, 10th, and 20th cycle, respectively.

The formation of MnO₂ (PDF#84-1713) was deposited at gasket in cathode position with increasing cycles, as displayed in Fig. S11. The MnO₂ is derived from the electro-oxidation of Mn²⁺ in aqueous electrolyte.



Fig. S12. The optical photographs of the gasket in assembled zinc ion battery without NMO electrode (Left image is after cycling and the right is initial state).

A special battery was assembled without NMO electrode. As shown in Fig.S12, the colour of the gasket on the positive side turns black in compared with the initial state, further illustrating the increased capacity in first 10 cycles.

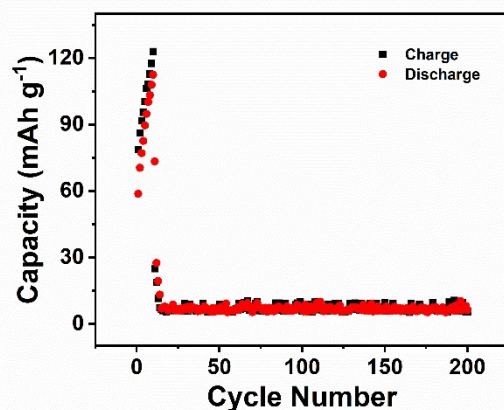


Fig. S13. The electrochemical performance at 0.1 A g⁻¹ (the first 10 cycles) and 4.0 A g⁻¹ of the assembled special battery based on the NMO electrode without washing.

The electrochemical performance of the NMO electrode without any washing was measured. The specific capacity of Zn/NMO without washing quickly decreases from 122.9 mAh g⁻¹ at 0.1 A g⁻¹ to 24.8 mAh g⁻¹ at 4.0 A g⁻¹, as shown in Fig. S13. The irreversible capacity decay of Zn/NMO battery is ascribed to the residual inorganic metal ions in NMO materials, restricting the intercalation/ deintercalation of H⁺ and Zn²⁺ in electrochemical process. Therefore, the washing condition plays an important role in achieving the high-performance Zn/NMO battery with the residual NH₄⁺.

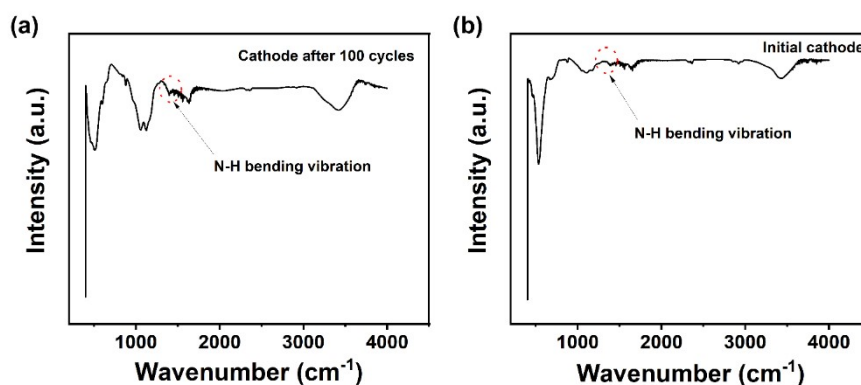


Fig. S14. The FT-IR spectra of a) cycled NMO cathode and b) initial NMO cathode.

As shown in Fig. S14, it is noted that there is an obvious peaks located at 1400 cm⁻¹ in FT-IR spectrum, which is ascribed to the N-H bending vibration of NH₄⁺ in MnO₂ even after 100 cycles at 4.0 A g⁻¹. It is in good agreement with the initial characterized N-H bending in FT-IR spectrum of NMO, suggesting the reversible presence of NH₄⁺ in MnO₂ after charge/discharge process.

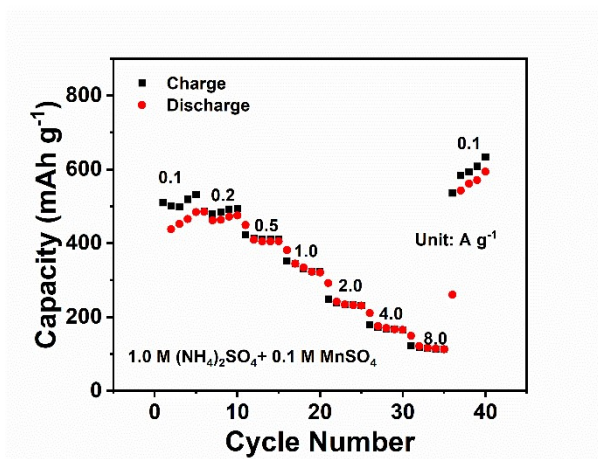


Fig. S15. Rate performance of the NMO-based battery in 1.0 M $(\text{NH}_4)_2\text{SO}_4$ + 0.1 M MnSO_4 .

The ZnSO_4 was replaced by $(\text{NH}_4)_2\text{SO}_4$ and was utilized in aqueous zinc ion battery to further confirm the electrochemical reversibility of NH_4^+ in charging and discharging process. As displayed in Fig. S15, the assembled NMO-based zinc ion battery with 1.0 M $(\text{NH}_4)_2\text{SO}_4$ and 0.1 M MnSO_4 electrolyte delivers a good electrochemical performance.

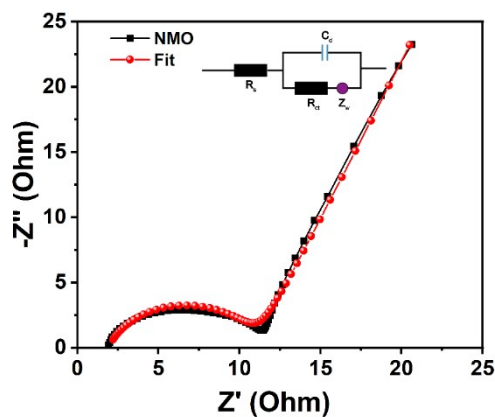


Fig. S16. Nyquist plot of the battery assembled with NMO electrode.

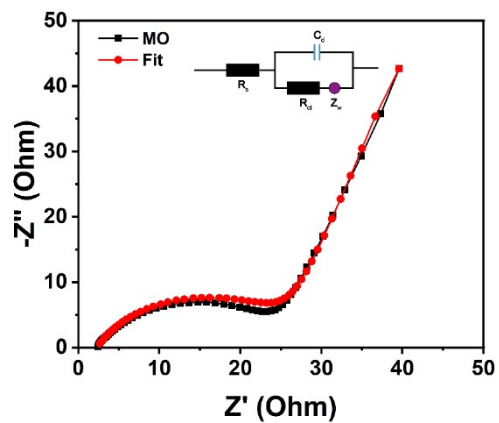


Fig. S17. Nyquist plot of the battery assembled with MO electrode.

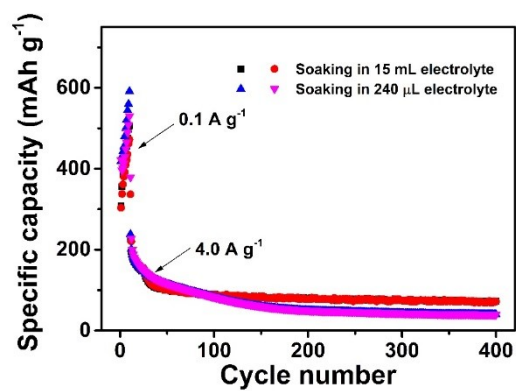


Fig. S18. The cycling stability of the Zn/NMO battery after soaking in different electrolyte for 24 h.

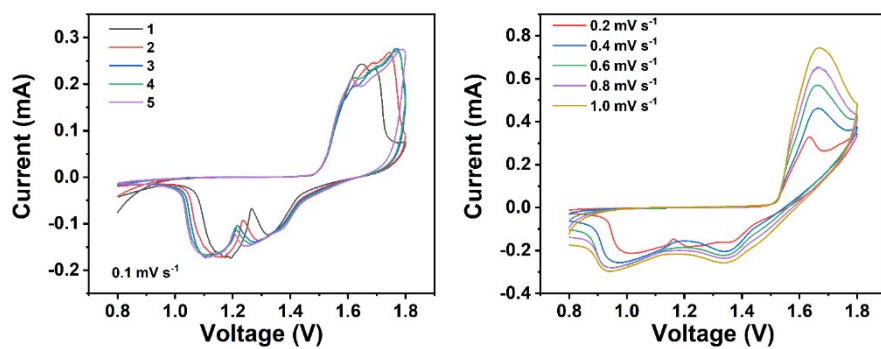


Fig. S19. CV curves of Zn/MO battery at different scan rates (0.1 to 1.0 mV s^{-1}).

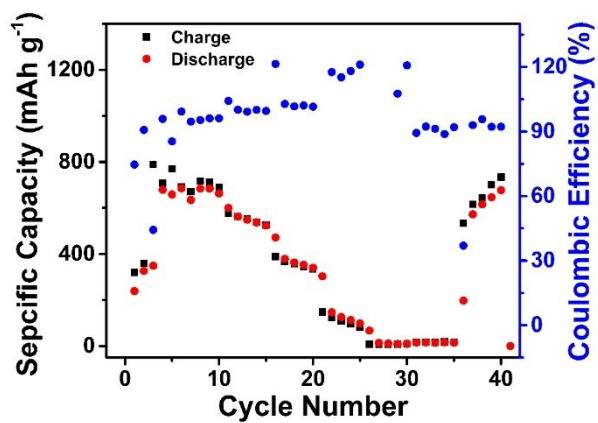


Fig. S20. Rate performance of Zn/MO battery at different current densities.

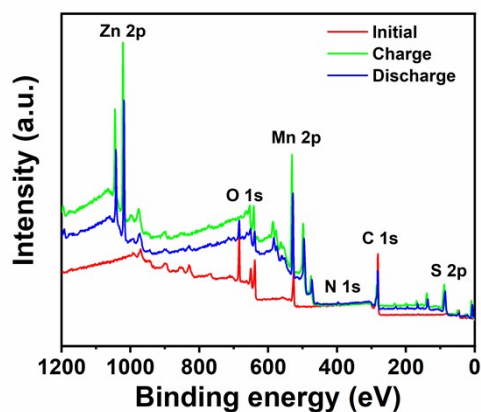


Fig. S21. The XPS spectra of NMO at different charge/discharge states.

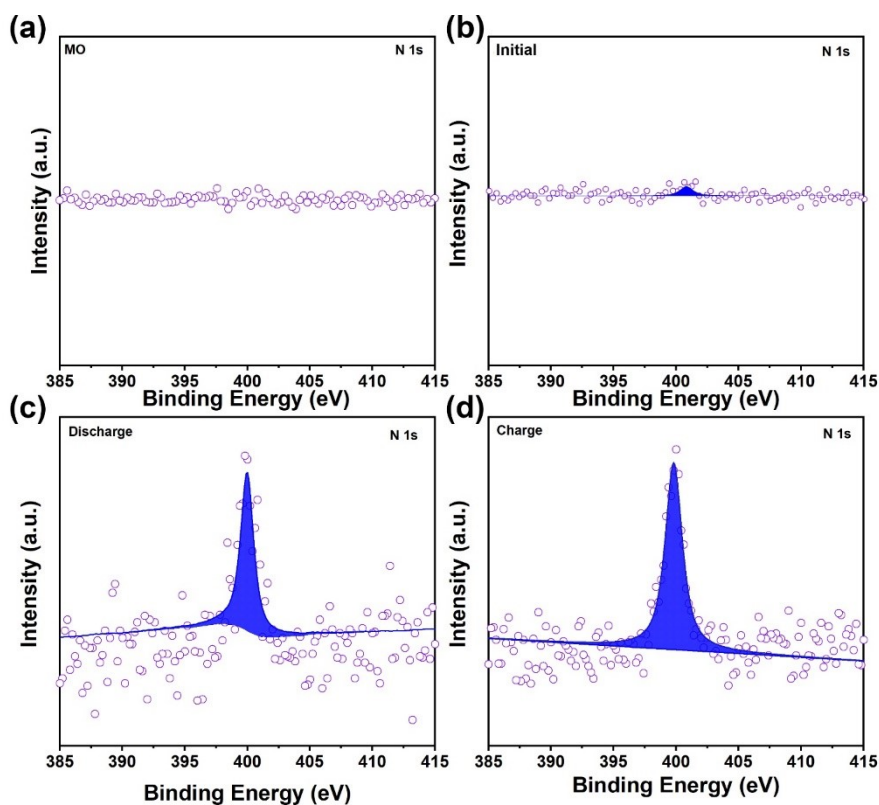


Fig. S22. The high-resolution N 1s XPS spectra. a) MO at initial state. b-d) NMO at initial, full charge, and full discharge states, respectively.

The increased intensity of N 1s XPS spectrum is ascribed to the extra exposed surface of NMO due to the reversible conversion of Mn element.

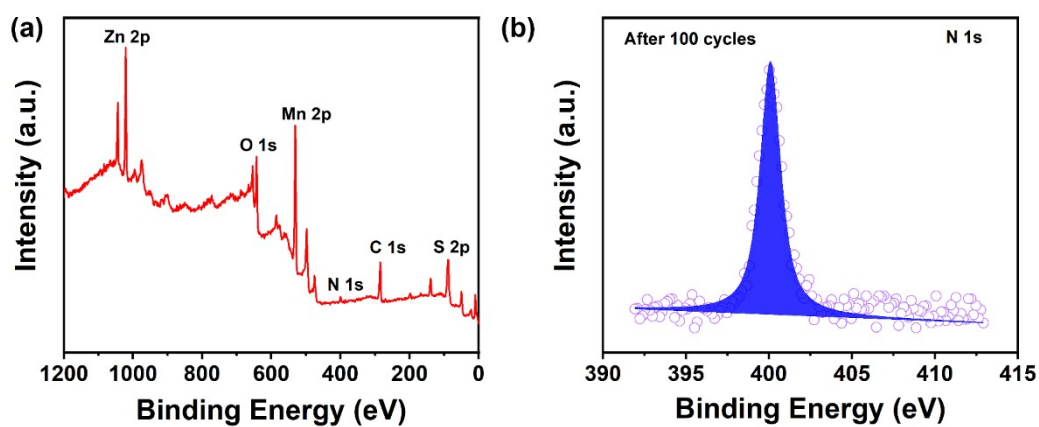


Fig. S23. a) The XPS spectra of NMO electrode and b) its high-resolution N 1s XPS spectrum after 100 cycles at 4.0 A g^{-1} .

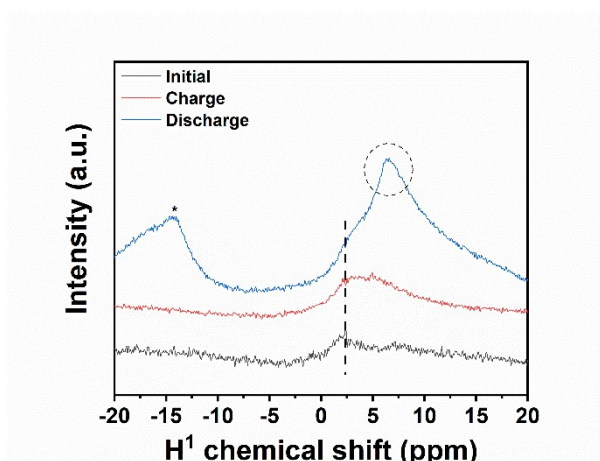


Fig. S24. The solid state ^1H NMR spectra of the NMO cathodes at different states.

The peak marked by * is the spinning side bands of isotropic peaks.

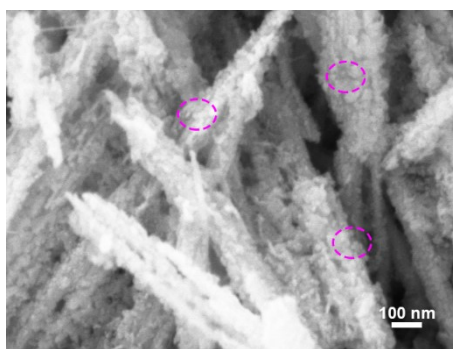


Fig. S25. SEM image of NMO electrode at fully-discharged state and the spot-like particles are the existence of ZnMn_2O_4 .

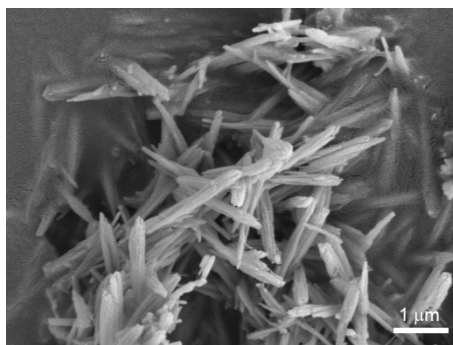


Fig. S26. SEM image of NMO at fully-charged state after 2500 cycles.

Table S1. Comparison of electrochemical performances of Zn/MnO₂ batteries.

Cathode	Capacity (mAh g ⁻¹)	Rate performance (mAh g ⁻¹)	Cycles	Capacity retention (mAh g ⁻¹)	Reference
γ -MnO ₂ /graphene	301 (0.5 A g ⁻¹)	95.8 (10 A g ⁻¹)	300	64.1%	[1]
MnO ₂ /graphene	317 (0.1 A g ⁻¹)	112 (7.5 A g ⁻¹)	2000	0.011% (capacity decay) (2.0 A g ⁻¹)	[2]
α -MnO ₂	~345 (0.1 A g ⁻¹)	~110 (2.0 A g ⁻¹)	100	~100 (0.5 A g ⁻¹)	[3]
β -MnO ₂ /C	~130 (0.1 A g ⁻¹)	40 (2.0 A g ⁻¹)	300	100 (0.3 A g ⁻¹)	[4]
MnO ₂	450 (0.1 A g ⁻¹)	95 (0.5 A g ⁻¹)	160	290 (0.2 A g ⁻¹)	[5]
MnO ₂	300 (0.308 A g ⁻¹)	120 (3.08 A g ⁻¹)	2000	100 (3.08 A g ⁻¹)	[6]
Li ₂ Mn ₂ O ₄	300 (0.1 A g ⁻¹)	75 (2.0 A g ⁻¹)	2000	69.5 (2.0 A g ⁻¹)	[7]
β -MnO ₂	375 (0.1 A g ⁻¹)	21 (2.0 A g ⁻¹)	1000	110 (0.2 A g ⁻¹)	[8]
MnO ₂	~365 (0.5 A g ⁻¹)	121 (4.0 A g ⁻¹)	4000	115 (4A g ⁻¹)	[9]
F-doping β -MnO ₂	320 (0.1 A g ⁻¹)	165 (2.0 A g ⁻¹)	150	~275 (0.5 A g ⁻¹)	[10]
Defective- MnO _{2-x}	330.2 (0.154 A g ⁻¹)	120 (3.08 A g ⁻¹)	3000	101.9 (1.85 A g ⁻¹)	[11]
Defect-MnO ₂	290 (0.3 A g ⁻¹)	134 (3.0 A g ⁻¹)	1000	~200 (1.0 A g ⁻¹)	[12]
Ce doping-MnO ₂	~260 (0.154 A g ⁻¹)	134 (1.54 A g ⁻¹)	100	~80 (1.54 A g ⁻¹)	[13]
Ti ₃ C ₂ T _x @MnO ₂	301.2 (0.1 A g ⁻¹)	202.2 (2.0 A g ⁻¹)	2000	~183 (2.0 A g ⁻¹)	[14]
PANI-intercalated MnO ₂	280 (0.2 A g ⁻¹)	110 (3.0 A g ⁻¹)	200	280 (0.2 A g ⁻¹)	[15]
PPy/MnO _{2-x}	302.0 (0.15 A g ⁻¹)	159.9 (3.0 A g ⁻¹)	1000	113.7 (6.0 A g ⁻¹)	[16]
NMO	457.4 (0.1 A g⁻¹)	164.5 (8.0 A g⁻¹)	10 000	42.7 (8.0 A g⁻¹)	This work

2. References

- [1] C. Wang, Y. Zeng, X. Xiao, S. Wu, G. Zhong, K. Xu, Z. Wei, W. Su, X. Lu, *J. Energy Chem.* **2020**, *43*, 182.
- [2] J. Wang, J. G. Wang, H. Liu, Z. You, Z. Li, F. Kang, B. Wei, *Adv. Funct. Mater.* **2020**, *31*, 2007397.
- [3] X. Gao, H. Wu, W. Li, Y. Tian, Y. Zhang, H. Wu, L. Yang, G. Zou, H. Hou, X. Ji, *Small* **2020**, *16*, 1905842.
- [4] W. Jiang, X. Xu, Y. Liu, L. Tan, F. Zhou, Z. Xu, R. Hu, *J. Alloy. Comp.* **2020**, *827*, 154273.
- [5] Q. Zhao, X. Huang, M. Zhou, Z. Ju, X. Sun, Y. Sun, Z. Huang, H. Li, T. Ma, *ACS Appl. Mater. Interfaces* **2020**, *12*, 36072.
- [6] J. Li, Y. Chen, J. Guo, F. Wang, H. Liu, Y. Li, *Adv. Funct. Mater.* **2020**, *30*, 2004115.
- [7] T. Zhang, Y. Tang, G. Fang, C. Zhang, H. Zhang, X. Guo, X. Cao, J. Zhou, A. Pan, S. Liang, *Adv. Funct. Mater.* **2020**, *30*, 2002711.
- [8] W. Liu, X. Zhang, Y. Huang, B. Jiang, Z. Chang, C. Xu, F. Kang, *J. Energy Chem.* **2021**, *56*, 365.
- [9] S. Wang, Z. Yuan, X. Zhang, S. Bi, Z. Zhou, J. Tian, Q. Zhang, Z. Niu, *Angew. Chem. Int. Ed.* **2021**, *60*, 7056.
- [10] S. Kim, B. R. Koo, Y. R. Jo, H. R. An, Y. G. Lee, C. Huang, G. H. An, *J. Mater. Chem. A* **2021**, *9*, 17211.
- [11] J. Zhao, Z. Xu, Z. Zhou, S. Xi, Y. Xia, Q. Zhang, L. Huang, L. Mei, Y. Jiang, J. Gao, Z. Zeng, C. Tan, *ACS Nano* **2021**, *15*, 10597.
- [12] J. Wang, J. G. Wang, X. Qin, Y. Wang, Z. You, H. Liu, M. Shao, *ACS Appl. Mater. Interfaces* **2020**, *12*, 34949.
- [13] J. Wang, X. Sun, H. Zhao, L. Xu, J. Xia, M. Luo, Y. Yang, Y. Du, *J. Phys. Chem. C* **2019**, *123*, 22735.
- [14] M. Shi, B. Wang, C. Chen, J. Lang, C. Yan, X. Yan, *J. Mater. Chem. A* **2020**, *8*, 24635.
- [15] J. Huang, Z. Wang, M. Hou, X. Dong, Y. Liu, Y. Wang, Y. Xia, *Nat. Commun.* **2018**, *9*, 2906.
- [16] Z. Li, Y. Huang, J. Zhang, S. Jin, S. Zhang, H. Zhou, *Nanoscale* **2020**, *12*, 4150.